



NRC Publications Archive Archives des publications du CNRC

A mass transport and hydrodynamic evaluation of membrane separation cell

Kawachale, Nikhil; Kirpalani, Deepak M.; Kumar, Ashwani

This publication could be one of several versions: author's original, accepted manuscript or the publisher's version. / La version de cette publication peut être l'une des suivantes : la version prépublication de l'auteur, la version acceptée du manuscrit ou la version de l'éditeur.

For the publisher's version, please access the DOI link below. / Pour consulter la version de l'éditeur, utilisez le lien DOI ci-dessous.

Publisher's version / Version de l'éditeur:

<https://doi.org/10.1016/j.cep.2009.08.001>

Chemical Engineering and Processing, 49, 7, pp. 680-688, 2010-07-01

NRC Publications Record / Notice d'Archives des publications de CNRC:

<https://nrc-publications.canada.ca/eng/view/object/?id=ed884684-779f-4583-933e-f358767b5d13>

<https://publications-cnrc.canada.ca/fra/voir/objet/?id=ed884684-779f-4583-933e-f358767b5d13>

Access and use of this website and the material on it are subject to the Terms and Conditions set forth at

<https://nrc-publications.canada.ca/eng/copyright>

READ THESE TERMS AND CONDITIONS CAREFULLY BEFORE USING THIS WEBSITE.

L'accès à ce site Web et l'utilisation de son contenu sont assujettis aux conditions présentées dans le site

<https://publications-cnrc.canada.ca/fra/droits>

LISEZ CES CONDITIONS ATTENTIVEMENT AVANT D'UTILISER CE SITE WEB.

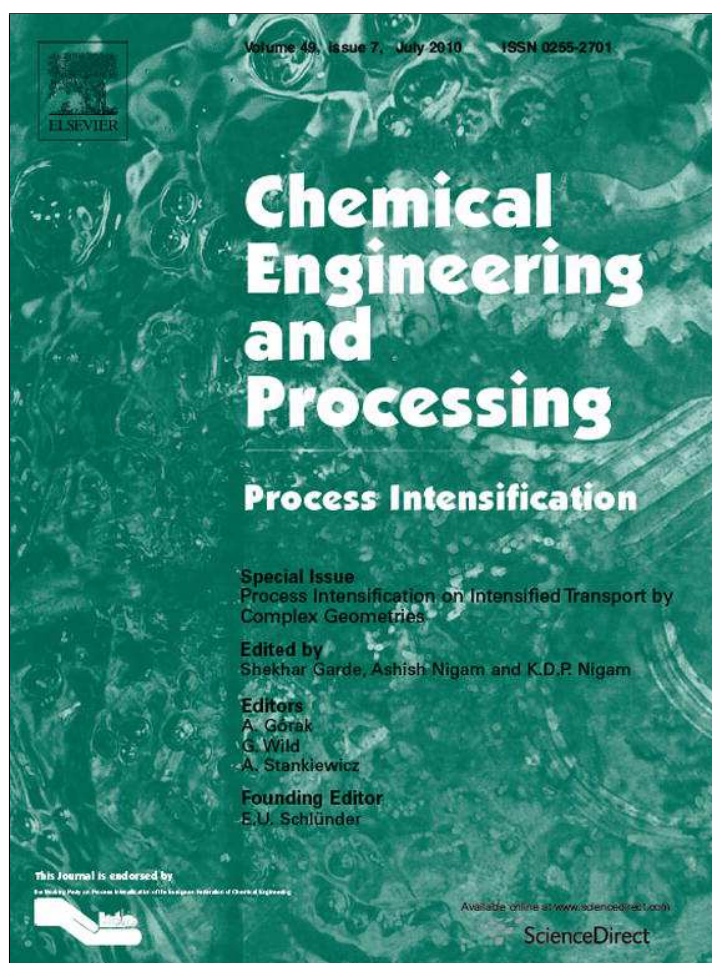
Questions? Contact the NRC Publications Archive team at

PublicationsArchive-ArchivesPublications@nrc-cnrc.gc.ca. If you wish to email the authors directly, please see the first page of the publication for their contact information.

Vous avez des questions? Nous pouvons vous aider. Pour communiquer directement avec un auteur, consultez la première page de la revue dans laquelle son article a été publié afin de trouver ses coordonnées. Si vous n'arrivez pas à les repérer, communiquez avec nous à PublicationsArchive-ArchivesPublications@nrc-cnrc.gc.ca.



Provided for non-commercial research and education use.
Not for reproduction, distribution or commercial use.



This article appeared in a journal published by Elsevier. The attached copy is furnished to the author for internal non-commercial research and education use, including for instruction at the authors institution and sharing with colleagues.

Other uses, including reproduction and distribution, or selling or licensing copies, or posting to personal, institutional or third party websites are prohibited.

In most cases authors are permitted to post their version of the article (e.g. in Word or Tex form) to their personal website or institutional repository. Authors requiring further information regarding Elsevier's archiving and manuscript policies are encouraged to visit:

<http://www.elsevier.com/copyright>



Contents lists available at ScienceDirect

Chemical Engineering and Processing: Process Intensification

journal homepage: www.elsevier.com/locate/cep

A mass transport and hydrodynamic evaluation of membrane separation cell[☆]

Nikhil Kawachale, Deepak M. Kirpalani, Ashwani Kumar*

Institute for Chemical Process and Environmental Technology, National Research Council of Canada, Ottawa, K1A0R6 Canada

ARTICLE INFO

Article history:

Received 8 June 2009

Received in revised form 13 July 2009

Accepted 2 August 2009

Available online 7 August 2009

Keywords:

Computational fluid dynamics (CFD)

Poly(dimethylsiloxane) membrane

Poly(ethersulfone) membrane

PEG(polyethylene glycol)

Membrane cell

Mass transfer

ABSTRACT

This study reports an analysis of membrane permeance and mass transfer coefficient in laboratory test cells for gas separation using computational fluid dynamics. Mass transfer coefficients and species concentration were computed across the membrane surface for gas mixture. The same test cells were examined for the fluid hydrodynamics in liquid separation. It was observed that the uniform flow distribution in the case of gas separation was responsible for improved permeance; whereas, a uniform flow had no significant effect on permeation rate for liquid separation. Also, the potential reasons for the difference in gas and liquid separation are discussed.

© 2009 Published by Elsevier B.V.

1. Introduction

The performance of laboratory membranes is evaluated in laboratory test cells over a range of operating conditions such as feed composition, flow rate, and pressure. Solute retention, concentration polarization and hydrodynamic profile are all significant and often independent factors. In membrane cell design, the hydrodynamics of test cells should be well defined so that other concurrent effects can be de-coupled in a clear manner, thus allowing a direct means for assessing the intrinsic mass transport properties of the test membrane. In this regard, it is desirable to have a laboratory membrane test cell with uniform flow distribution above the permeating area of membrane for evaluating its performance. The benefits of uniform flow distribution over the test membrane sample are the reliability of its characterization data for estimation of membrane system scale up. However, in practice it is difficult to accomplish the above characteristics due to design complexities combined with mass transfer. A detailed investigation of fluid flow pattern in a test cell provides fundamental information for membrane based separations. In our earlier study [1] based on hydrodynamics of membrane separation cell, it was found that the geometry of a test cell played an important role in terms of membrane performance for binary feed gas mixture of oxygen and nitrogen (O₂/N₂). However, in the study, average permeance across the membrane area and velocity profiles were considered for the

evaluation of cell performance. Furthermore, the study was limited to gas separation and did not address issues relating to liquid separation. Ideally, mass transport together with fluid dynamics along the membrane could be better represented by mass transfer coefficient or Sherwood number. Therefore, a detailed mass transport analysis in the immediate vicinity of membrane was desirable in order to evaluate separation properties based on local concentration of species. More accurate estimation of mass transfer properties at the membrane surface with cross-flow for a range of empirical conditions can be achieved through a more efficient design that implements uniform distribution. Computational fluid dynamics (CFD) simulation methods have been applied to gain an understanding of the fluid flow behavior in membrane modules [2]. The coupled CFD approach can model the mass-flow through mathematical coupling of the species continuity and momentum in a compressible solver with defined permeances [3]. In addition, CFD simulations can provide the flexibility to construct computational models that could be easily adapted to wide variety of physical conditions without the requirement to construct a prototype of the test cell, thus offering an effective virtual prototyping at a relatively low cost. Literature on design of such a module, especially intended for separation utilizing flat membrane, is limited. In previous work, Belfort [4] reviewed the use of fluid dynamics in membrane systems. Robert et al. [5] attempted to produce uniform hydrodynamics condition for plate and frame module by means of video camera. Design improvement such as relocating the outlet of hollow fiber membrane module was reported by Harada [6]. In their technical note, Tarabara and Wiesner [7] demonstrated that the geometry of module was an important factor in the enhancement of membrane performance. The flow was found to be unidirectional

[☆] NRCC No.:51720.

* Corresponding author. Tel.: +1 613 998 0498; fax: +1 613 991 2384.

E-mail address: ashwani.kumar@nrc-cnrc.gc.ca (A. Kumar).

over most of the channel area with the exceptions of the channel corners and the stagnated areas were observed in the dead ends at the inlet and outlet of channel. Their work showed that it was possible to improve membrane module geometry by using CFD results to predict distribution. Darcovich et al. [8] designed a thin channel cross-flow module for the characterization of flat ceramic membranes. A total of ten variables were considered for the module designs, which were used to evaluate the predicted module performance for each combination of their design. Three-dimensional modeling of flows in spacer-filled channels with modified flat and annular channels was reported by Ranade and Kumar [9]. In this work, the spacers were designed to create directional changes in the flow to reduce concentration polarization and membrane fouling. Zydney and Xenopoulos [10] examined the mass transport phenomena involving Dextran[®] permeation for ultrafiltration membranes. The study was conducted to examine the use of a stirred cell and a parallel plate tangential flow device with varying filtrate flux, stirring speed and feed flow rate and concluded that the stirred cell provided more accurate test results. An interesting study on membrane fouling and fluid velocity profile in various geometries by means of mapping of protein fouling has been reported by Delaunay et al. [11]. This work described ultrafiltration of skimmed milk in two different module geometries and validated the results with CFD. Feron et al. [12] proposed a novel test cell for gas separations. This test cell was intended for characterization of high flux flat sheet membrane with uniform mass transfer over the membrane area and the cell design was verified with numerical simulation. However, in their work the membrane was assumed to be an impermeable wall and mass transfer across the membrane was neglected in numerical procedures. Abdel-jawad et al. [13] studied the flow zones on feed and permeate sides of molecular sieve membrane. This membrane was modeled with CFD by creating a bounded region separating the feed and permeate sides of membrane. The gas transport phenomenological equations were solved in a bounded region to obtain continuum flows on both sides without accounting for the flow profiles in feed/permeate-volumes. However, a comprehensive fluid dynamics study in order to outline design aspects of membrane separation cell, that considers both gas and liquid separations independently along with actual mass transport across the membrane has not yet been reported in literature.

The objective of this study is to evaluate the overall effect of gas separation membrane cell design modifications in terms of mass transfer coefficients and to define an average Sherwood number across the membrane, in order to investigate the effect of suggested membrane cell geometry modifications on liquid separation process. This involved the development of a mass transport model to improve the performance prediction from earlier gas separation studies. Flow profiles of liquid feed solution for improved membrane cell have been simulated with CFD using empirical results.

2. Experimental

2.1. Membrane test cell

One of the aspects of present study is to examine the reported geometry of membrane cell together with different design elements and relate it to fluid hydrodynamics of liquid separation. Accordingly, the conventional test cell that has been reported in our earlier work [1] was considered for further evaluation. The generic separation cell as shown in Fig. 1(a) and (b); which fundamentally resembles other typical membrane cells used in laboratories was constructed of stainless steel and consists of feed-volume (top) and permeate-volume (base) as two different components. The membrane was supported by a Millipore[®] porous metal screen

to facilitate the permeate flow. These components were sealed together using two different O-rings and a placement metal ring with cap-screws and flat washers as shown in Fig. 1. In Fig. 1, the conical shaped feed-channel had one feed-inlet and a retentate-outlet, both 3.18×10^{-3} m in diameter were opposite to each other and profiled at an angle of 32° to x -axis. The cylindrical shaped permeate-channel mainly comprised of a porous metal support, was rested on a plate with series of holes to hold the membrane and facilitate the permeate flow through a permeate-outlet of 3.18×10^{-3} m diameter. The membrane with an effective area of 1.1×10^{-3} m² physically divided the feed-volume from the permeate-volume and was supported by porous metal screen.

2.2. Simulation conditions

In present work, the numerical and mass transport studies for gas separation process were based on experimental results reported in our previous work [1] on flow distribution of gas feed mixture at constant pressure and concentration. The membrane, used in this work for gas permeation experiments, was comprised of highly microporous polysulfone support coated with a 0.2 μ m thick poly(dimethylsiloxane) (PDMS) layer. Also, the membrane was reported to be selective for O₂ and the same was considered as a probe gas together with an industrial grade (0.1) air as a gas feed mixture.

A poly(ethersulfone) membrane with polypropylene backing was utilized for liquid separation CFD studies and empirical validation. The membrane is hydrophilic and has a suitable molecular weight cut-off (1 kDa) so that it partially retains the solutes and allows the permeation of solvent. A 200 ppm solution of polyethylene glycol and distilled water (PEG-600/H₂O) was used as liquid feed solution. The experimental setup for liquid separation was a standard constant-pressure permeation system, as reported by Hazlett et al. [14]. The liquid feed solution was allowed through feed-inlet at constant pressure and concentration and the desired flow rate was achieved through flow controllers before entering the membrane cell. The retentate stream was maintained at nearly the same pressure as feed-inlet and was expelled from the retentate-outlet. The permeate mass through membrane together with retentate stream were allowed to flow through individual lines and were periodically sampled to measure composition. Shimadzu Scientific Instruments (Columbia, MD) TOC-VCSH total organic carbon analyzer was utilized to determine PEG-600 concentrations in the test samples. The volumetric flow meters and control valves were supplied by King Instruments Company (Huntington, CA) and The Swagelok[®] Company (Solon, OH), respectively. The experimental conditions were maintained at steady state with laminar flow ($125 < Re < 1500$) at feed-inlet, and ambient temperature (22 °C). Also, based on the empirical data for gas [1] and liquid separation, it was determined that the plasticization and fouling effects can be neglected and the partitioning of selective species (O₂ or H₂O) from the bulk feed to the membrane cannot be considered as mass transfer limiting.

3. Numerical methodology for liquid separation

3.1. Governing equations

In order to simulate the flow of Newtonian fluid through a membrane cell, the basic equations of fluid mechanics were combined with boundary conditions representing a membrane wall. These governing equations based on conservation for mass and momentum were solved using finite volume method. In addition, a set of species conservation equations was solved to account for the separation. The equations, based on the physical principles of continuity,

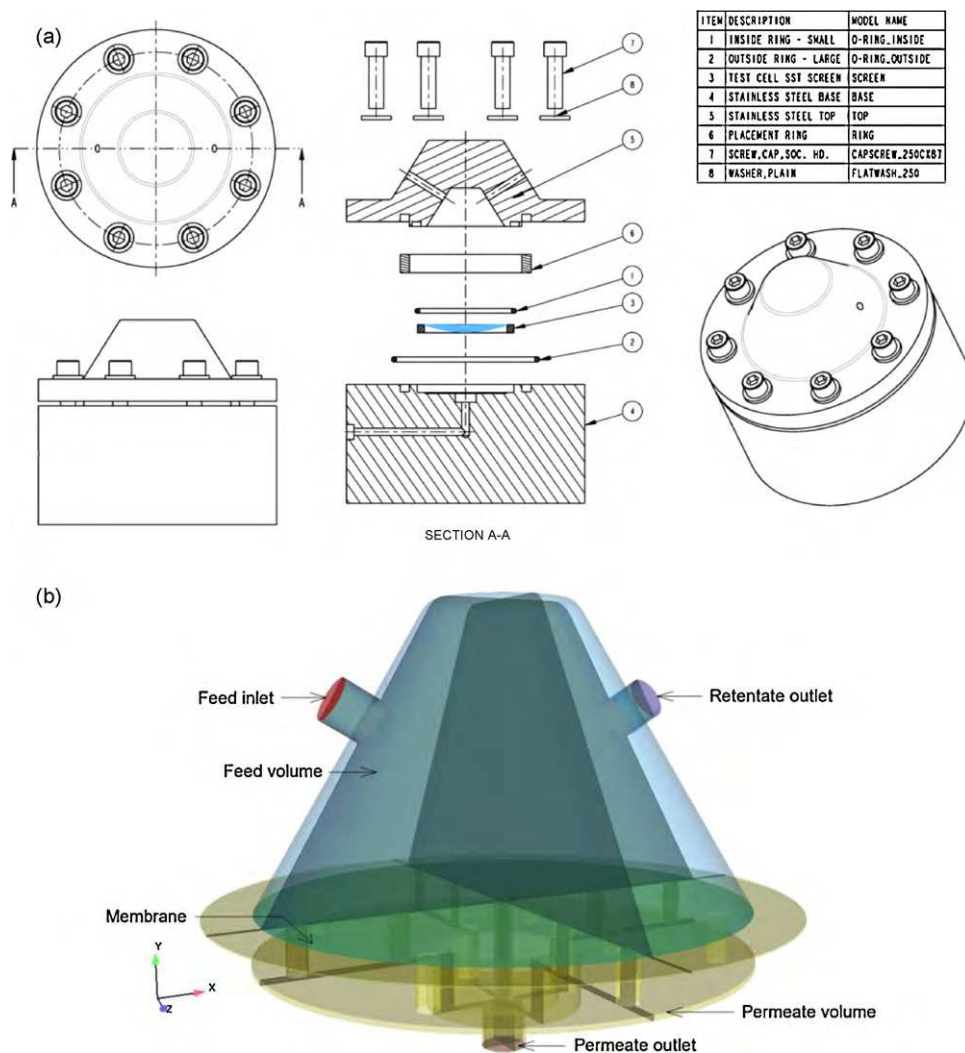


Fig. 1. (a) Sectional view and components of conventional cell and (b) fluid geometry of convectional cell domain together with virtual surfaces intersecting x and y-axis, and z and y-axis.

momentum conservation and solutes conservation were solved for a three-dimensional (3D) domain for laminar flow with unsteady state operation [3].

3.2. Boundary conditions

Model development and simulations were performed in FLUENT® 6.3 CFD software. All the functions required to compute a solution and to display the results were accessible either through an interactive interface or by including user defined functions. The properties of feed stream were defined before executing the simulation loop. Operating parameters, such as flow rate, pressure and species concentrations were obtained and implemented as boundary conditions from empirical data. The simulations were performed using unsteady-laminar flow conditions at an ambient temperature. The discretization of governing equations was performed using a segregated compressible flow solver in which each governing equation was solved separately. Given that the velocities obtained earlier might not satisfy the continuity equation locally, pressure–velocity coupling was used to obtain the necessary pressure and velocity corrections along with the face mass fluxes in such a way that the continuity equation was satisfied. Semi-Implicit Method for Pressure-Linked Equations (SIMPLE) formulation was set as a part of pressure–velocity coupling algorithm

[15]. Non-slip boundary conditions at wall surface and variation in species concentration were included in the compressible solver as well.

In order to update the velocity field, the 3D Navier-Stokes equations were solved using new values for cell nodal pressures and face mass fluxes. The discrete velocities and pressures were stored in cell centers by a non-staggered system, which consisted of cells and faces. The fluid properties were updated based on the previous iterations or given initial values. The convergence criteria for the continuity and velocity parameters were fixed to 0.001%. Higher convergence criterion ($1.0 \times 10^{-7}\%$) was set for the selective species to offer sufficient iterations for complete convergence between the boundary and the interior mesh grid. In order to obtain a stable solution, the under relaxation factors, which limit the influence of the previous iteration over the present one were fixed to 0.3 for the pressure, 0.9 for density, 0.6 for the momentum and 0.9 for species. Lower values of under relaxation factors were selected for pressure and momentum to prevent oscillating solutions [16]. Pressure was set to 'Pressure Staggering Option' (PRESTO!) and momentum, density and mass fractions were set to 'Second Order Upwind' discretization schemes for more accurate results. 'Aggressive Advanced Multigrid' (AMG) scheme had been applied to accelerate the convergence of the solver by computing corrections on a series of coarse grid levels. The AMG cycle type for

the coupled equation for pressure, momentum and species concentration was set to fixed 'F-Cycle' as a recursive procedure. Also, 'Biconjugate Gradient Stabilized Method' (BCGSTAB) was employed to solve non-symmetrical linear systems to avoid the frequent irregular convergence patterns [16].

3.3. Flow domain and grid generation

The dimensions of the computational domain were identical with that of the membrane separation cell that has been described earlier. GAMBIT® 2.3 preprocessing software was used to generate the 3D geometry and mesh for CFD studies. An effort was made to implement the structured, uniform quad/hex grid for the entire geometry for numerical advantage. In order to accomplish this, the geometry was decomposed in such a way that quad/hex scheme could be accomplished for all the segments of complex portions. The choice of Map and Cooper scheme resulted in an increase in the relative amount of hexahedral elements and hence rendered an efficient mesh with low overall skewness (EquAngle Skew < 0.8) throughout the domain. Structured meshing was performed to divide the flow domain in to sub-domains and hexahedral cells and the discretized governing equations were solved inside each cell. The continuity and momentum equations across the common interfaces between two sub-domains (feed/permeate-volumes) were solved to visualize fluid flow in the entire domain. Also, grid refinement was performed to achieve grid independence by analyzing the concentration gradient within the geometrical domain. The membrane cell computational geometry consisted of a mass-flow inlet, boundary for introducing the feed stream and pressure outlets for retentate and permeate flows. The membrane in the domain was defined as shadowed wall while all other walls represented the barriers of the remaining cell geometry. In order to examine species concentration and velocity magnitude near the membrane surface, virtual edges across x-axis and virtual surfaces along x and z-axis were generated numerically at a distance of one computational cell (1.02×10^{-4} m) on both sides of the membrane. Also, an intersecting virtual surface was generated across x and y-axis in order to visualize flow characteristics within the flow domain of membrane cell.

3.4. User defined functions (UDF)

The transport of gas across the membrane was achieved using a series of user defined functions in FLUENT® software. Membrane modeling was addressed by incorporating permeabilities and mass fluxes as the UDF written in 'C code' [3]. The issue of hydraulic jump across the membrane was resolved by patching the cells from upper and lower zones with two different values of initial pressures. The 'Define Profile' macro was used in parallel with the adjacent cell index to link the relation between the hydrodynamics and the membrane transport phenomena. Changes in the fluid flow adjacent to the membrane interface were accounted for by the UDF with the prediction of new parameters for membrane wall along with the shadow side. Additionally, the UDF updated the solver data with new parameters at the membrane wall.

The source and sink terms in the UDF for gas separation were calculated by using the simple relationship between the linear flux and the driving force, which is commonly described by Fick's law in membrane separations:

$$J_i = -D_i \frac{dC_i}{dN} \quad (1)$$

In the case of liquid separation, the source and sink terms in UDF were calculated by using the relationship that is known as Darcy's law. The governing equations discussed earlier, were added to Darcy's equation in the form of transport equations and the

source/sink terms in UDF were calculated accordingly:

$$J_i = P_i(P - \pi) = \frac{1}{\mu \eta_i} (P - \pi) \quad (2)$$

4. Results and discussion

4.1. Membrane cell evaluation for gas separation

A summary of previous work [1] on gas separation process is provided to describe the new findings. The results of the CFD simulation for gas separation are shown as the vectors of velocity magnitude at low feed-inlet flow rate (0.108×10^{-5} m³/s) in Fig. 2(a) and (b). It is obvious that the flow in conventional cell was not well-distributed in the flow direction as maximum velocity occurs on the far-side of the cell rather than a uniform distribution. Other possible design shortcomings identified were the short circuiting of some of the gas feed mixture to retentate-outlet without having any contact with the membrane that could have a significant impact on the performance of the membrane cell. As shown in Fig. 2(b) that the flow was relatively well-distributed in the modified cell over the entire membrane surface without any non-uniformities [1]. Also, any possible short circuiting in the conventional cell was eliminated in the modified configuration. It was also observed that the modified cell showed an improved over-

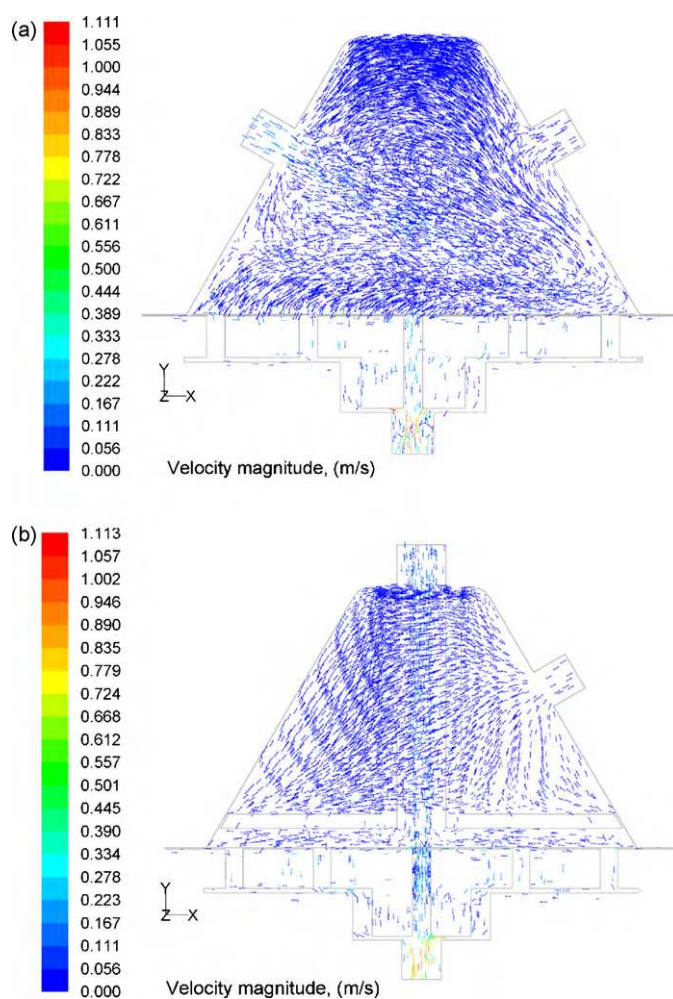


Fig. 2. Velocity magnitude vectors of gas separation for feed-inlet flow rate 0.108×10^{-5} m³/s at virtual surface intersecting x and y-axis: (a) conventional cell and (b) modified cell [1].

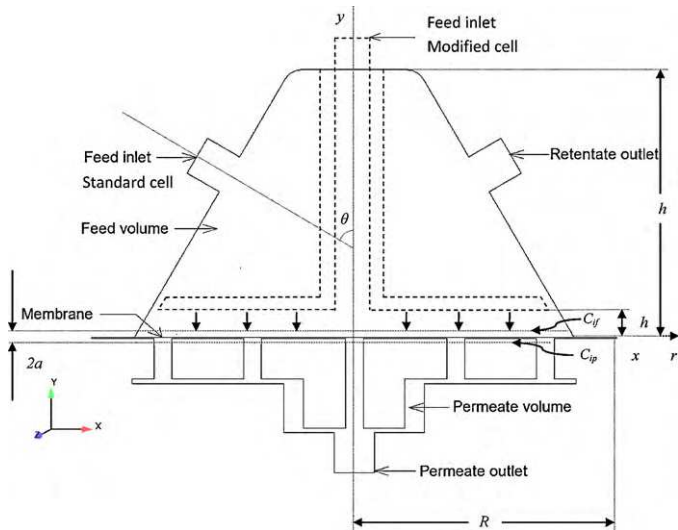


Fig. 3. Schematic view of conventional membrane separation cell together with modified feed-inlet configuration at intersecting x and y-axis.

all performance than the conventional cell and the performance increments were more notable for the low feed-inlet flow rates ($Q_f < 0.432 \times 10^{-5} \text{ m}^3/\text{s}$). In order to understand the detailed flow structures of gas feed mixture and their impact on cell performance, variation in mass transfer coefficient in the membrane vicinity was further explored. Figs. 2(a), (b) and 3 provide the schematics of regular and modified membrane cells described in Section 2 for subsequent discussion in this work.

4.2. Mass transfer model across the membrane for gas separation

The permeance in membrane separation processes is a pressure normalized flux through the membrane and is considered as a parameter to measure the separation performance. However, permeance accounts for an average mass transport through entire membrane rather than considering local transport rate that may vary based on geometrical configuration of the membrane separation cell. Ideally, mass transfer along with fluid dynamics in the membrane separation should be represented by coupling film theory with an empirical correlation that yield the mass transfer coefficient or Sherwood number as a function of the Reynolds and Schmidt numbers in the immediate membrane vicinity. In order to gain a better understanding of the limitations discussed above and to evaluate the mass transfer phenomenon near the membrane surface, empirical data of gas separation reported in our previous study [1] was considered. The schematic of reported conventional membrane cell geometry together with suggested modifications are shown in Fig. 3. The steady state incompressible fluid flow through feed-volume (frustum) can be considered as a cylindrical flow across the y-axis. This condition could be better represented by a developed Poiseuille flow and based on this hypothesis the formulation for mass transport model in the immediate membrane vicinity can be described as follows.

Steady state mass transfer in the immediate vicinity across the x-axis of membrane is governed by convective diffusion equation [17]:

$$\frac{\partial^2 C_i^*}{\partial y'^2} = f(y^*) \frac{\partial C_i^*}{\partial x^*} \quad (3)$$

where C_i^* , x^* and y^* are dimensionless variables and can be defined as:

$$C_i^* \equiv C_i^*(x^*, y^*) \equiv \frac{C_i - C_{if}}{C_{ip} - C_{if}} \quad (4)$$

$$x^* \equiv \frac{R}{Re Sc h \cos \theta} \quad (5)$$

$$y^* \equiv \frac{y'}{h \cos \theta} \quad (6)$$

In this configuration, the boundary conditions are as follows:

$$C_i^*(0, y^*) = 1$$

$$C_i^*(x^*, -1) = 0$$

As a result, the local mass transport coefficient is represented as:

$$k_d(x^*) = k_d(r) = -\frac{D_i}{\bar{C}_i(x^*) - C_{if}} \left(\frac{\partial C_i}{\partial y'} \right)_{y=-a} \\ = -\frac{D_i C_{ip} - C_{if}}{a \bar{C}_i(x^*) - C_{if}} \left(\frac{\partial C_i^*}{\partial y^*} \right)_{y^*=-1} \quad (7)$$

where $\bar{C}_i(x^*)$ is the bulk concentration at x^* . Hence, the mean mass transport coefficient is then obtained as:

$$\bar{k}_d = \frac{1}{\pi R^2} \int_0^R (2\pi r) k_d(r) dr = \frac{1}{\pi x^{*2}} \int_0^{x^*} k_d(x^{*2}) dx^* \quad (8)$$

From which the average Sherwood number can be calculated as:

$$\bar{S}_h = \frac{\bar{k}_d(2R)}{D} \quad (9)$$

In order to illustrate mass transport phenomenon in the immediate membrane vicinity on the permeate side; species concentration and mass transfer coefficient were shown as a function of membrane diameter. As shown in Fig. 4(a) and (b), permeate concentration of O_2 is plotted against the membrane diameter across the x-axis and at a virtual line below the membrane for different feed-inlet flow rates for conventional cell and modified cell, respectively. As shown in Fig. 4(a), the permeate concentration profiles of O_2 for all feed-inlet flow rates are offset towards left in conventional cell as a result of improper feed-inlet configuration and this phenomenon is more significant at higher feed-inlet flow rates ($Q > 0.432 \times 10^{-5} \text{ m}^3/\text{s}$). However, in the case of modified cell the concentration profiles of O_2 for the range of feed-inlet flow rates are relatively well-distributed across the x-axis as shown in Fig. 4(b). Moreover, it is clear from Fig. 4(b) that there is a significant drop in O_2 concentration at the center for modified cell. This phenomenon, which is more prominent at lower feed-inlet flow rates ($Q < 0.432 \times 10^{-5} \text{ m}^3/\text{s}$), could be related to the modified feed-inlet configuration. Considering that the actual height of feed-volume (h) in the modified cell is much lower than that of a conventional cell, higher velocities at feed-inlet opening above the membrane results in an even distribution of gas mixture over the membrane surface. The plots of oxygen concentration in the immediate vicinity and below the membrane for both membrane cells confirm the CFD results observed in our earlier study [1].

Based on the mass transport model, local mass transfer coefficient of O_2 is plotted against the membrane diameter and at a virtual line across the x-axis above the membrane for different feed-inlet flow rates in the case of both conventional and modified cells as shown in Fig. 5(a) and (b), respectively. It can be observed from the plots of local mass transfer coefficient for different feed-inlet flow rates in Fig. 5(a) that the overall profile is not well-distributed over the membrane surface and is shifted towards the left side of the x-axis as a result of an improper feed-inlet configuration as

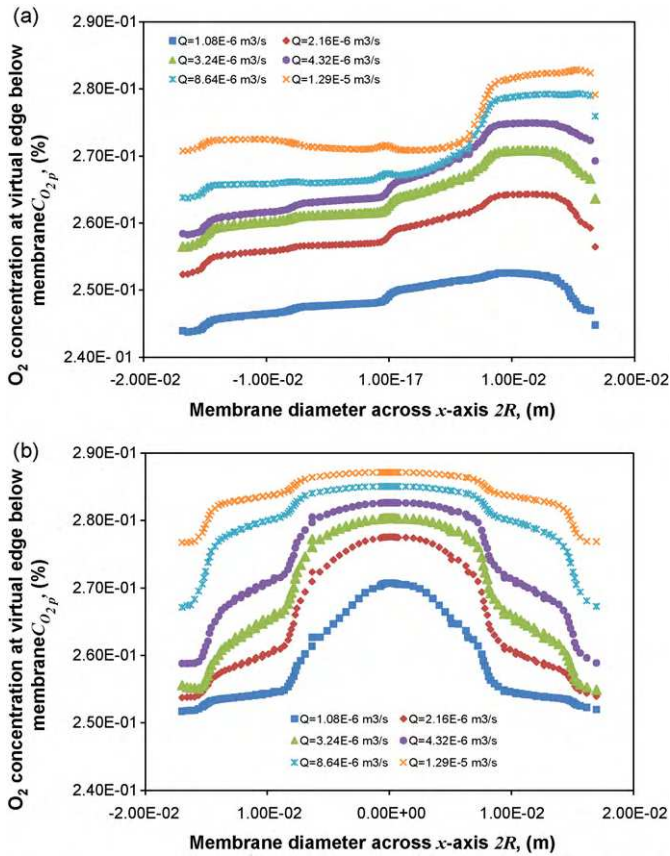


Fig. 4. Concentration profiles of O₂ at virtual line across the x-axis below the membrane for different feed-inlet flow rates (Q): (a) conventional cell and (b) modified cell.

reported in the previous study [1]. As shown in Fig. 5(b), the trend for local mass transfer coefficient is more uniform in the modified cell. Also, an overall mass transport for the range of feed-inlet flow rates is higher in the modified cell in comparison with a conventional cell. Moreover, it can be seen from Fig. 5(b) that at lower feed-inlet flow rates ($Q < 4.32 \times 10^{-5} \text{ m}^3/\text{s}$), there is a significant drop in mass transfer coefficient profiles at the center of membrane for the modified cell. As discussed earlier, this phenomenon is more evident at lower flow rates and could be a result of lower velocity at the opening of modified feed-inlet configuration. It is interesting to note that the velocity profiles were comparable with the contour plots for velocity magnitude as shown in Fig. 10(b) [1]. In addition, it can be clearly observed from Fig. 4(a) and (b), and Fig. 5(a) and (b) that the local mass transfer coefficient and concentration of species are related and at any feed-inlet flow rate they are inversely proportional with each other in both the conventional and modified cells.

The range of operating conditions together with comparison of the O₂ permeance and an average Sherwood number are shown in Tables 1 and 2 for the conventional and modified cells, respectively.

Table 1
Experimental and numerical results obtained for conventional cell.

Feed-inlet flow rate (m ³ /s)	O ₂ permeance (m ³ /(s m ² Pa))	\bar{S}_h
1.08E-06	2.95E-09	4.07E+01
2.17E-06	3.14E-09	4.95E+01
3.25E-06	3.25E-09	5.52E+01
4.33E-06	3.34E-09	5.93E+01
8.65E-06	3.43E-09	6.50E+01
1.30E-05	3.49E-09	6.78E+01

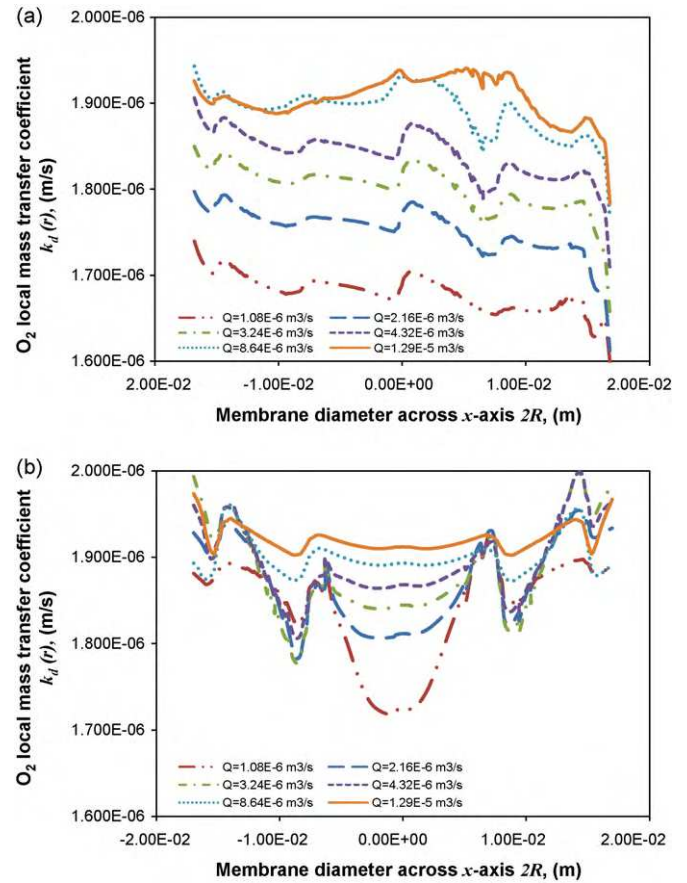


Fig. 5. Profiles of $k_d(r)$ for O₂ at virtual line across the x-axis above the membrane for different feed-inlet flow rates (Q): (a) conventional cell and (b) modified cell.

It is obvious from the data that an increase in Sherwood number for the modified cell was associated with an increase in O₂ permeance. Also, based on the results of mass transfer model it can be concluded that the local mass transfer coefficient or Sherwood number represent the transport phenomena in the immediate membrane vicinity more rigorously as compared to the conventional 'permeance' parameter in order to define performance of a membrane based separation process.

4.3. Flow profile of test cells for liquid separation

In order to validate the effects of modified feed-inlet configuration, the simulations for liquid separations were performed at two different empirical pressures (4.4×10^5 and 7.9×10^5 Pa) and at a constant flow rate ($5 \times 10^{-5} \text{ m}^3/\text{s}$) at feed-inlet. CFD results using actual 3D geometry of the conventional cell were compared with experimentally measured boundary parameters. As shown in Table 3, it was observed that in case of both conventional and modified cells, the PEG-600 concentrations estimated by numerical procedure at permeate-outlet and for two different empirical

Table 2
Experimental and numerical results obtained for modified cell.

Feed-inlet flow rate (m ³ /s)	O ₂ permeance (m ³ /(s m ² Pa))	\bar{S}_h
1.08E-06	3.32E-09	5.74E+01
2.17E-06	3.41E-09	6.13E+01
3.25E-06	3.45E-09	6.32E+01
4.33E-06	3.49E-09	6.50E+01
8.65E-06	3.53E-09	6.68E+01
1.30E-05	3.58E-09	6.90E+01

Table 3
Comparison between experimental and numerical PEG-600 concentrations at permeate-outlet for different feed-inlet pressures for conventional and modified cells.

Feed-inlet pressure (Pa) $\times 10^5$	$C_{\text{PEG-600p}}$, (%) $\times 10^{-4}$, experimental	$C_{\text{PEG-600p}}$, (%) $\times 10^{-4}$, numerical
Conventional cell		
4.4	1.09	1.09
7.9	1.16	1.16
Modified cell		
4.4	1.04	1.04
7.9	1.09	1.09

pressures were in good agreement with experimentally measured entities as reported in our previous work [1] for gas separation. Moreover, the theoretical CFD results for the fluxes have been validated with empirical results without significant error for both separation cells. Therefore, it can be concluded that the CFD based modeling approach is capable of closely predicting the flow distribution in membrane based liquid separation processes.

4.3.1. Flow distribution in conventional cell

The overall flow distribution within the test cell was examined based on the vectors of velocity magnitude, which were plotted alongside the virtual surface intersecting the flow domain at x and y -axis. Fig. 6 shows the results of CFD simulation for liquid separation in terms of the velocity magnitude vectors at a feed-inlet pressure of 4.4×10^5 Pa. It is clear from Fig. 6 that for liquid feed solution, the flow mal-distribution is less significant in the flow direction as the highest velocity occurs in the central zone, which is in contrast to the results observed for the gas feed mixture [1]. Also, a possible shortcoming of short circuiting of the feed stream to retentate-outlet without having any contact with the membrane, which was identified in the gas separation is evident in Fig. 6 for liquid separation as well and can be related to the restricted performance of the membrane cell.

A contour plot of velocity magnitude for liquid separation at 4.4×10^5 Pa feed-inlet pressure and at a virtual surface in the immediate vicinity above the membrane for the conventional cell is shown in Fig. 7(a). A similar contour plot from earlier study [1] for the gas feed mixture at a feed-inlet flow rate of $0.108 \times 10^{-5} \text{ m}^3/\text{s}$ is shown in Fig. 7(b) for comparison purpose. It can be seen from Fig. 7(b) that for gas separation the flow distribution is skewed towards retentate side in the conventional cell. However, it can be observed from Fig. 7(a) that in comparison with gas separation

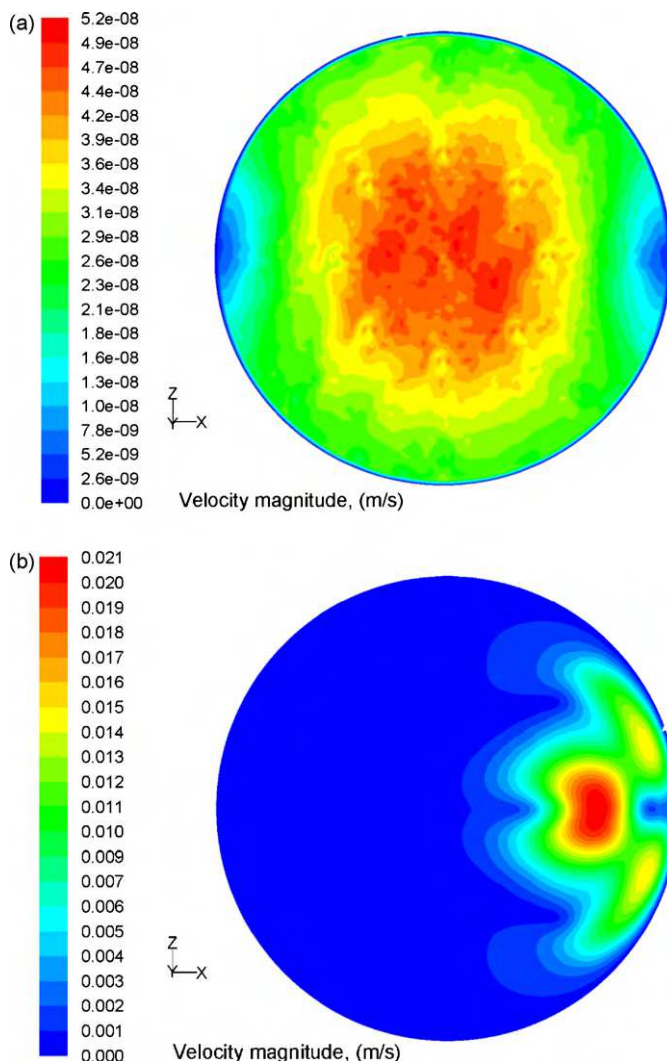


Fig. 7. Contours plot of velocity magnitude in the immediate vicinity at virtual surface intersecting x and z -axis above the membrane for the conventional cell: (a) liquid separation at feed-inlet pressure 4.4×10^5 Pa and (b) gas separation at feed-inlet flow rate $0.108 \times 10^{-5} \text{ m}^3/\text{s}$ [1].

the flow distribution is more uniform over the membrane surface for the liquid feed solution.

4.3.2. Flow distribution in modified cell

A modified feed-inlet configuration was proposed in our previous study [1] in order to achieve uniform flow distribution over the membrane surface. As shown in Figs. 3 and 8, the feed-inlet in the modified cell that is profiled at an angle in conventional cell is shifted on the top of the feed-volume at an angle of 90° to x -axis and is extending just above the membrane ($h = 1.02 \times 10^{-5} \text{ m}$). A diffuser disk was fabricated around the feed-inlet pipe in order to prevent any possible short circuiting of the feed stream without being in contact with the membrane. The optimum distance between the diffuser disk/feed-inlet and the membrane was obtained by analyzing CFD results for improved performance without significant change in pressure difference between the feed-inlet and retentate-outlet for the experimental range at similar flow conditions [1]. It should be noted that the permeate-volume was kept unchanged as a result of very low flow rates on the permeate side of the membrane.

The velocity magnitude vectors across the intersecting virtual surface along x and y -axis in the modified cell and at a feed-inlet pressure of 4.4×10^5 Pa are shown in Fig. 9 for the liquid separation.

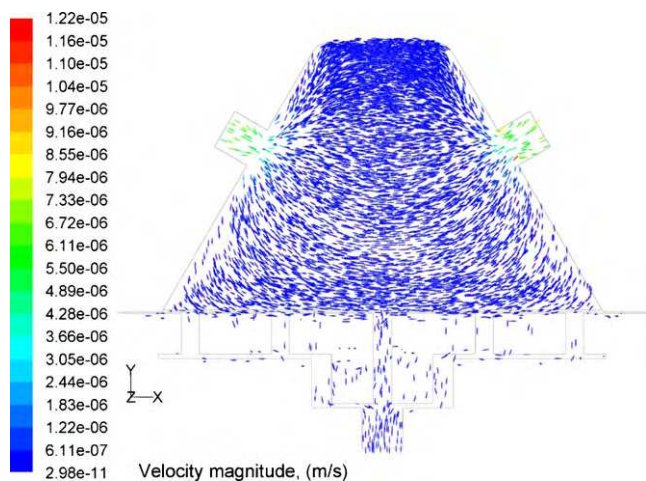


Fig. 6. Velocity magnitude vectors of liquid separation in the conventional cell for feed-inlet pressure 4.4×10^5 Pa at virtual surface intersecting x and y -axis.

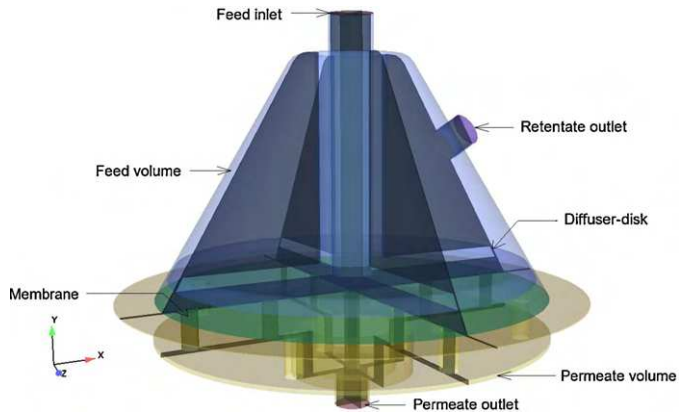


Fig. 8. Fluid geometry of modified cell domain together with virtual surfaces intersecting x and y-axis, and z and y-axis.

Comparing Fig. 9 with Fig. 6, it can be observed that for liquid separation the flow mal-distribution in the flow direction is reduced in the case of modified cell. Moreover, the possible limitation of short circuiting of the feed stream to retentate-outlet without having any contact with the membrane, which was present in conventional cell is nonexistent in the modified cell. The numerical result of modified cell for the liquid feed solution at 4.4×10^5 Pa feed-inlet pressure, represented by contour plots for velocity vectors at a virtual surface in the immediate vicinity and above the membrane, is shown in Fig. 10(a). A similar contour plot for the gas separation at feed-inlet flow rate of $0.108 \times 10^{-5} \text{ m}^3/\text{s}$ from our earlier work [1] is shown in Fig. 10(b). Comparing Figs. 7(a) and 10(a), it can be seen that the liquid flow distribution has improved in the modified cell as a result of modified feed-inlet configuration; however the improvements in flow distribution are not as significant as in the case of gas separation process (Figs 7(b) and 10(b)).

4.4. Flow distribution and permeation performance of liquid separation

In order to compare the performance of conventional and modified cells, the effects of feed-inlet configurations on velocity magnitude are shown in Fig. 11 for liquid separations. Fig. 11 compares the velocity magnitude in the immediate vicinity at a virtual edge across the x-axis and above the membrane for conventional and modified feed-inlet configurations. It can be clearly observed

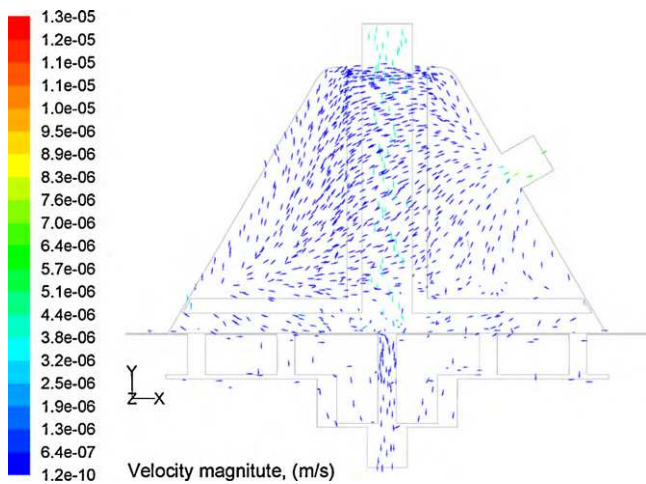


Fig. 9. Velocity magnitude vectors for the modified cell for liquid separation at feed-inlet pressure 4.4×10^5 Pa at virtual surface intersecting x and y-axis.

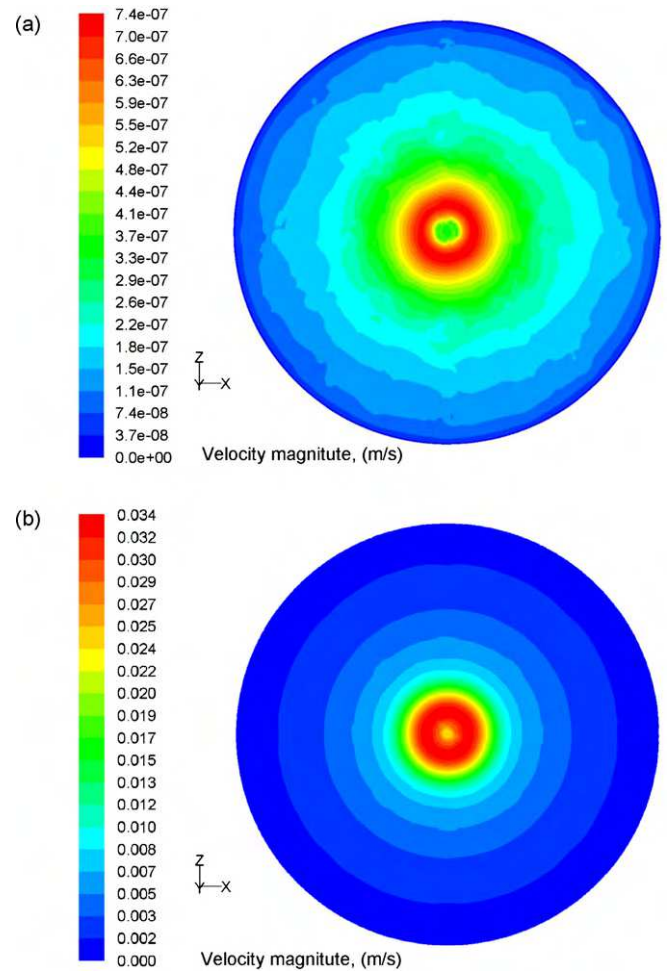


Fig. 10. Contours plot of velocity magnitude in the immediate vicinity at virtual surface intersecting x and z-axis above the membrane for the modified cell: (a) liquid separation at feed-inlet pressure 4.4×10^5 Pa and (b) gas separation at feed-inlet flow rate $0.108 \times 10^{-5} \text{ m}^3/\text{s}$ [1].

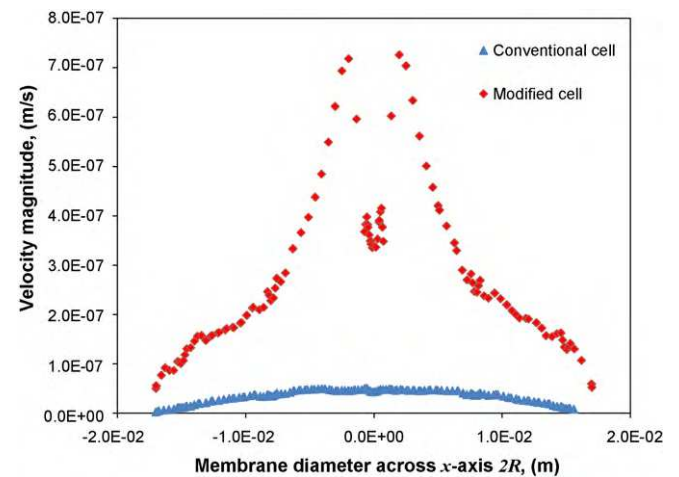


Fig. 11. Comparison of velocity magnitude at virtual line across the x-axis just above the membrane for liquid separation at feed-inlet pressure 4.4×10^5 Pa.

from Fig. 11 that for the same feed-inlet pressure the modified cell has higher velocities and more uniform distribution over the membrane as compared to the conventional cell. However, in spite of the improved velocity distribution and an elimination of possible short circuiting of feed stream, the observed performance improvements in liquid separation were less significant as compared to the gas separation.

This observation could be explained by significantly different intrinsic liquid properties such as the density and the viscosity, which are higher than gases. Obviously, in the case of liquid feed solution higher viscosity and density contributes to more even dispersion of fluid within the test cell volume irrespective of the feed-inlet location. Also, very low concentration of trace component (PEG-600) in the liquid feed solution can be considered as another reason for insignificant performance changes in the case of liquid separation.

5. Conclusions

It was shown that the variation in the mass transfer coefficient and species concentration at different locations over the membrane in test cells can be studied using a CFD technique. The proposed model confirmed the flow profile observed in both conventional and modified cell geometries for previously reported work on gas separation. Also, it was observed that the mass transfer coefficient or Sherwood number represented the transport phenomena in immediate membrane vicinity more rigorously and provided an improved measure of membrane performance as compared to permeance alone. It was concluded that the poor distribution and possible short circuiting of flow in the feed-volume was due to an improper feed-inlet configuration in the gas separation process. However, the impact of previously proposed modifications for feed-inlet for improving the performance was not significant for the liquid separation process. The reason for this limitation could be significant difference in the physical properties of liquids and gases.

Appendix A. Nomenclature

a	distance between membrane and virtual line across x -axis
C	concentration, wt.%
C^*	dimensionless concentration
D	diffusion coefficient, m^2/s
$f(y^*)$	dimensionless velocity function
h	height of feed-volume
J	flux, $m^3/(m^2 s)$
$k_d(x^*)$	local mass transfer coefficient, m/s
\bar{k}_d	mean mass transfer coefficient, m/s
N	space coordinate normal to the section for component i
P	permeability, $m/(s Pa)$
P	trans-membrane pressure, Pa
Q	mass-flow, m^3/s
r	radial coordinate, m
R	membrane radius, m

Re	Reynolds number
S_c	Schmidt number
\bar{S}_h	mean Sherwood number
x^*	dimensionless distance parameter
y'	distance coordinate across y -axis
y^*	dimensionless coordinate across y -axis

Greek symbols

π	liquid feed solution osmotic pressure, Pa
μ	dynamic viscosity, $Pa s$
η	membrane resistance, m^{-1}

Subscripts

f	feed
p	permeate
i	species

References

- [1] N. Kawachale, A. Kumar, D.M. Kirpalani, A flow distribution study of laboratory scale membrane gas separation cells, *J. Membr. Sci.* 332 (2009) 81.
- [2] R. Ghidossi, D. Veyret, P. Moulin, Computational fluid dynamics applied to membranes: state of the art and opportunities, *Chem. Eng. Proc.* 45 (2006) 437.
- [3] N. Kawachale, A. Kumar, D.M. Kirpalani, Numerical Investigation of hydrocarbon enrichment of process gas mixtures by permeation through polymeric membranes, *Chem. Eng. Technol.* 31 (1) (2008) 58.
- [4] G. Belfort, Fluid mechanics in membrane filtration: recent developments, *J. Membr. Sci.* 40 (1989) 123.
- [5] J. Robert, R. Giinter, J. Hapke, Optimization of flow design in a plate type membrane module system by means of a video camera, in: R.A. Bakish (Ed.), *Proc. 4th Int. Conf. Pervaporation Processes Chem. Ind., Mater. Corp., Englewood Cliffs, NJ*, 1989, p. 554.
- [6] S. Harada, Hollow-fiber module container for reverse osmosis, *Japan Patent*, No. 60-261506 A2 (1985) 3.
- [7] V.V. Tarabara, M.R. Wiesner, Computational fluid dynamics modeling of the flow in a laboratory membrane filtration cell operated at low recoveries, *Chem. Eng. Sci.* 58 (2003) 239.
- [8] K. Darcovich, M.M. Dal-Cin, S. Balleve, J.P. Wavelet, CFD-assisted thin channel membrane characterization module design, *J. Membr. Sci.* 124 (1997) 181.
- [9] V.V. Ranade, A. Kumar, Comparison of flow structures in spacer-filled flat and annular channels, *Desalination* 191 (2006) 236.
- [10] A.L. Zydney, A. Xenopoulos, Improving Dextran tests for ultrafiltration membranes: effect of device format, *J. Membr. Sci.* 291 (2007) 180.
- [11] D. Delaunay, M. Rabiller-Baudry, J.M. Gozálviz-Zafrilla, B. Balanec, M. Frappart, L. Paugama, Mapping of protein fouling by FTIR-ATR as experimental tool to study membrane fouling and fluid velocity profile in various geometries and validation by CFD simulation, *Chem. Eng. Proc.* 47 (2008) 1106.
- [12] P. Feron, J.W. van Heuven, J.J. Akkerhuis, R. van der Welle, Design and development of a membrane test cell with uniform mass transfer: application to characterisation of high flux gas separation membranes, *J. Membr. Sci.* 80 (1993) 157.
- [13] M.M. Abdel-jawad, S. Gopalakrishnan, M.C. Duke, M.N. Macrossan, P. Smith Schneider, J.C. Diniz da Costa, Flowfields on feed and permeate sides of tubular molecular sieving silica (MSS) membranes, *J. Membr. Sci.* 299 (2007) 229.
- [14] J.D. Hazlett, T.A. Tweddle, O. Kutowy, in: M.I.H. Baird, S. Vijyan (Eds.), *Proc. 2nd Int. Con. Separations Sci. and Technol., Canadian Society for Chem. Eng., Ottawa, ON*, 1989, p. 65.
- [15] S.V. Patankar, *Numerical Heat Transfer and Fluid Flow*, Hemisphere Publishing Corp., Washington, DC, 1980.
- [16] User's Guide, *Fluent 6. 3 Documentation*, Fluent Inc., Lebanon, NH, 2006.
- [17] F. Coeuret, T.Z. Fahidy, Steady-state mass transport at stationery discs under divergent laminar radial flow conditions, *J. Appl. Electrochem.* 31 (2001) 671.